RSC Advances

PAPER

View Article Online
View Journal | View Issue

Cite this: *RSC Adv.*, 2018, **8**, 22974

Bent-core dimers with top-to-bottom linkage between central units†

Martin Horčic,[a] Jiří Svoboda,*[a] Vladimíra Novotná,[b] Damian Pociecha[c] and Ewa Gorecka[c]

Received 14th May 2018
Accepted 18th June 2018

DOI: 10.1039/c8ra04108c

rsc.li/rsc-advances

A structurally new type of core-to-core dimer with a top-to-bottom linkage between the central cores of bent molecules is presented. The structure of the bent-core molecules was modified by changing the length of the spacer between the central cores and terminal chains, by changing the type of linkage groups in the bent-core arms and by variation of the terminal chain polarity – introducing polyfluoroalkyl and oligosiloxane units. Additionally, the outer phenyl ring was substituted with three alkyl chains to mimic a polycatenar system. For all compounds the mesophase behaviour and structural parameters were established to gain information about the molecular structure–mesomorphic property relationship.

Introduction

Bent-core liquid crystals have become an integral part of the family of thermotropic liquid crystals (LC) in recent years.[1] The most important discovery concerns the fact that bent-core compounds with non-chiral molecules are able to pack into polar phases. The most frequently investigated mesophase is the tilted lamellar SmCP phase. In the SmCP phase, the bent molecules are packed in layers giving rise to the in-layer polar axis and therefore ferro- or antiferroelectric properties can be observed.[2–4] Four structures of the SmCP phase were distinguished (designated as $SmC_{S/A}P_{F/A}$) with synclinic (S) or anticlinic (A) molecular tilt and ferroelectric (F) or antiferroelectric (A) polar correlation between neighbouring layers. The chirality of the layers can alternate creating a racemic state, or can be the same in neighbouring layers forming homochiral domains. In addition to a nematic phase, orthogonal smectic A or columnar mesophases can be observed. The nomenclature for columnar phases, B_1 and B_{1REV}, has been introduced for non-switchable and switchable form, resp., of the mesophases formed from layer fragments.[5]

With rising attention LC bent-core dimers and oligomers have also been investigated for their diversity of mesomorphic properties in comparison with monomeric LCs.[6–27] In the molecular structure of dimers constituting mesogenic units are joined in various modes, the most frequently end-to-end,[6–9,12–16,27] and scarcely side-to-end[11] and top-to-top.[10] The mesomorphic properties of the end-to-end joined dimers are sensitive to the character of the spacer: materials with an alkylene spacer exhibited nematic and smectic phases[9–12] and columnar phases[13,14] depending on the length of the spacer, respectively. When the bent-core monomers were linked by an oligosiloxane and carbosilane unit, ferroelectric and antiferroelectric SmCP phases were observed for various number of siloxane units.[6,8,9] The same effect was proved at non-symmetrical dimers composed of a bent-core and rod-like units.[15,17–21,24] Few examples of columnar[19–21] and SmCP phases[22] typical for bent-shaped molecules were also found.

In our preliminary report[28] we have presented a new type of bent-core liquid crystalline dimers designed by a top-to-bottom connection of bent-core central units by a propylenedioxy linking unit. The studied compounds showed a strong dependence of mesomorphic properties on the length of the terminal alkyl chains. While the compounds with short chains (ethyl, butyl) exhibited the SmA phases, lengthening the arms to hexyl and octyl resulted in appearance of the columnar B_1 (Col_r) phase, and further lengthening to the decyl and dodecyl chain resulted in formation of the polar SmC_AP_A phases. In this contribution we present synthesis and systematic physical studies of this new type of top-to-bottom bent-core dimers with respect to the length of the alkylene spacer, type, length and number of the terminal chains, and type and orientation of linking groups.

Experimental

Synthesis of the studied compounds

General chemical formula of the studied compounds **Dm-n** is shown in Fig. 1. We have varied the length of the spacer (m), the

[a]Department of Organic Chemistry, University of Chemistry and Technology, CZ-166 28 Prague 6, Czech Republic. E-mail: Jiri.Svoboda@vscht.cz; Fax: +420220443688; Tel: +420220444288

[b]Institute of Physics of the Czech Academy of Sciences, Na Slovance 2, CZ-182 21 Prague 9, Czech Republic. E-mail: novotna@fzu.cz; Fax: +420286890527; Tel: +420266053111

[c]Laboratory of Dielectrics and Magnetics, Chemistry Department, Warsaw University, Al. Zwirki i Wigury 101, 02-089 Warsaw, Poland. E-mail: pociu@chem.uw.edu.pl; Fax: +48228221075; Tel: +48228221075

† Electronic supplementary information (ESI) available. See DOI: 10.1039/c8ra04108c

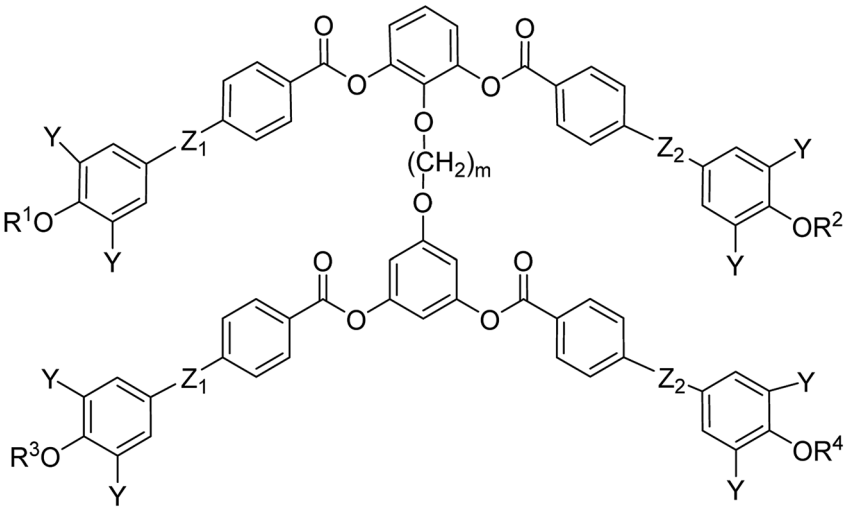

Fig. 1 General chemical formula of the studied top-to-bottom dimers **Dm-n**.

length and character of terminal chains (R^1, R^2, R^3 and R^4) and linkage groups in outer part of arms, Z_1 and Z_2. Additionally, in some materials instead of terminal alkyls we utilized polyfluorinated or siloxanylalkyl chains (will be specified later). As a linking groups (Z_1, Z_2) in the outer part of the bent-core molecules either ester groups with various orientation, photosensitive azo units were used, or two phenyl rings were joined directly (see Fig. 1). In the last series, the terminal benzene rings were substituted with multiple terminal chains (Y).

The detailed synthesis of the studied materials and characterisation of all compounds, *i.e.*, synthesis of cores, intermediates and target compounds of all series **Dm-n** is summarised in the ESI.†

Experimental methods

Differential scanning calorimetry (DSC) measurements were performed using Perkin-Elmer 7 calorimeter. The compounds 2–5 mg were hermetically sealed in aluminium pans and

Table 1 Mesomorphic properties of dimers **D4-n** with the butylenedioxy spacer[a]

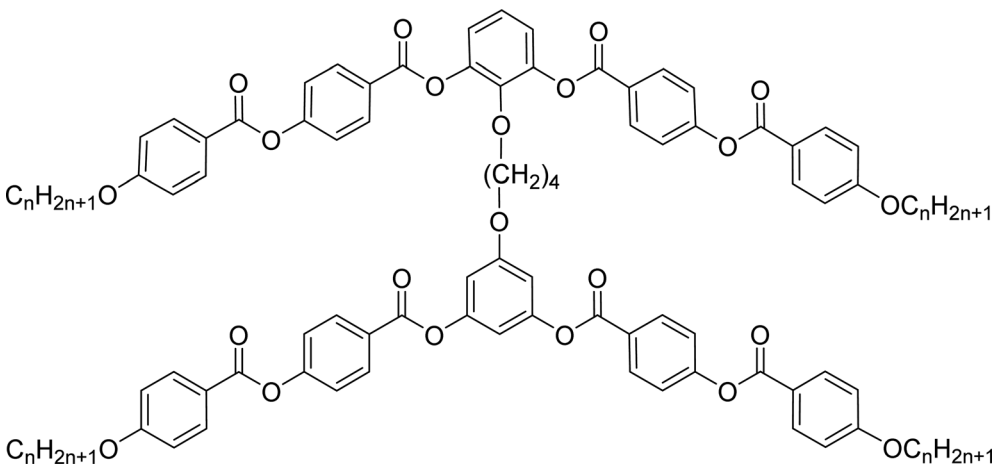

Comp.	*n*	mp [Δ*H*]	T_{cr} [Δ*H*]	M_1	T_{tr} [Δ*H*]	Iso
D4-2	2	203 [+53.6]	140 [−49.9]	SmA	207 [−28.5]	•
D4-4	4	163 [+40.9]	156 [−40.3]	SmA	186 [−27.8]	•
D4-6	6	153 [+31.5]	138 [−30.4]	SmA	159 [−31.9]	•
D4-8	8	154 [+68.3]	101 [−31.1]	B_1	136 [−19.8]	•
D4-10	10	122 [+49.4]	52 [−18.5]	SmC_AP_A	125 [−36.4]	•
D4-12	12	102 [+36.8]	49 [−25.5]	SmC_AP_A	134 [−40.4]	•

[a] Melting point, mp, phase transition temperatures, T_{tr}, and temperature of crystallization, T_{cr}, in °C, and corresponding enthalpy changes, Δ*H*, are in brackets in kJ mol^{-1}.

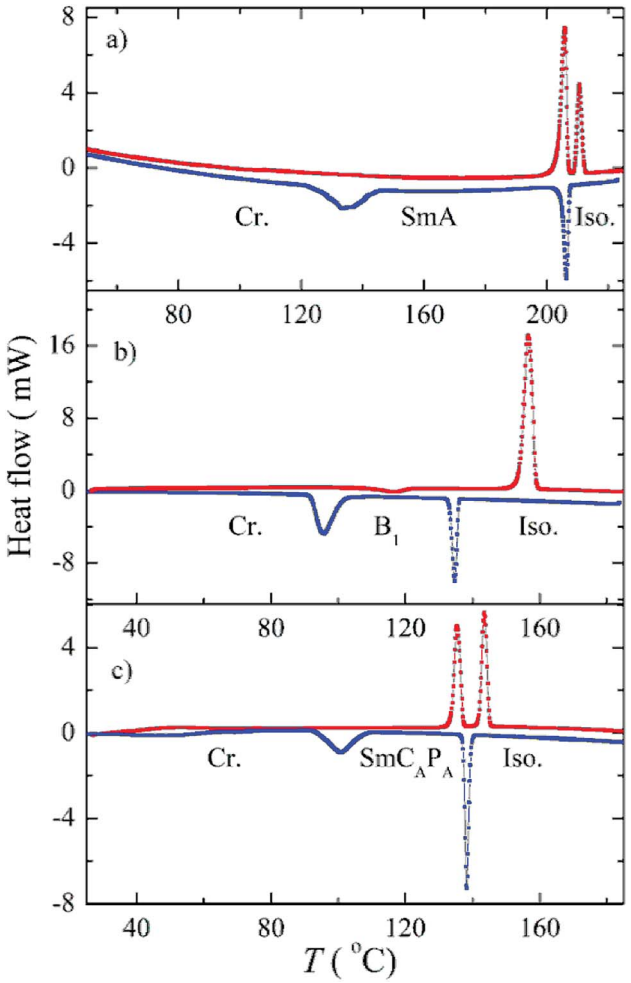

Fig. 2 DSC plots taken at the second heating (red) and the subsequent second cooling run (blue colour) for selected compounds: (a) **D4-2**, (b) **D4-8**, and (c) **D4-12**. Phases are designated in the corresponding temperature interval.

inserted into the calorimeter chamber, which was filled during measurements with nitrogen atmosphere. Temperature and enthalpy change values were calibrated on extrapolated onsets for melting points of water, indium and zinc. Mostly the calorimetric measurements were performed on heating and subsequent cooling runs at a rate of 5 K min^{-1}.

The phases were identified from textures observed under a polarizing optical microscope Nikon Eclipse E600Pol. The glass cells for texture observation and electro-optical studies were prepared from glasses with ITO transparent electrodes (5 × 5 mm^2) separated by two mylar sheets defining the cell thickness (usually of about 3 μm). The glass cells were filled with studied compounds in the isotropic (Iso) phase by capillary action. The Linkam LTS E350 heating/cooling stage was used, which enabled temperature stabilization within ±0.1 K.

The electro-optical properties have been studied using a driving voltage from generator Philips PM 5191, which was accompanied by an amplifier. The voltage of maximum amplitude ±200 V was provided for the measuring system and the digital oscilloscope Tektronix DPO4034 display the switching current *vs.* time. The dielectric spectroscopy was measured using a Schlumberger 1260 impedance analyser in the frequency range of 10 Hz to 10 MHz, at stabilized temperatures during frequency sweeps.

The X-ray diffraction studies were performed using Bruker Nanostar system with CuKα radiation (wavelength $\lambda = 1.5418$ Å), Vantec 2000 area detector, MRI TCPU H heating stage working in the transmission mode and Bruker GADDS system (CuKα radiation, Vantec 2000 area detector) working in reflection mode. In both systems the temperature stability was 0.1 K. Partially oriented samples for experiments in reflection were prepared as droplets on heated surface.

Mesomorphic properties

The role of the terminal alkyl chains length

In the previous manuscript we have reported a study of top-to-bottom dimers with the propylenedioxy spacer designated as **D3-n**.[28] We demonstrated that the increasing length of the terminal chains (R═C_nH_{2n+1}) resulted in variety of the mesophases formed, starting from the intercalated SmA for the shortest homologue through the columnar B_1 phase to the lamellar SmCP phases for the longest homologues. Herein we have prepared and studied homologues **D4-n** (the structure of materials is shown in the heading of Table 1) with the butylenedioxy spacer. We have modified the terminal chains length R

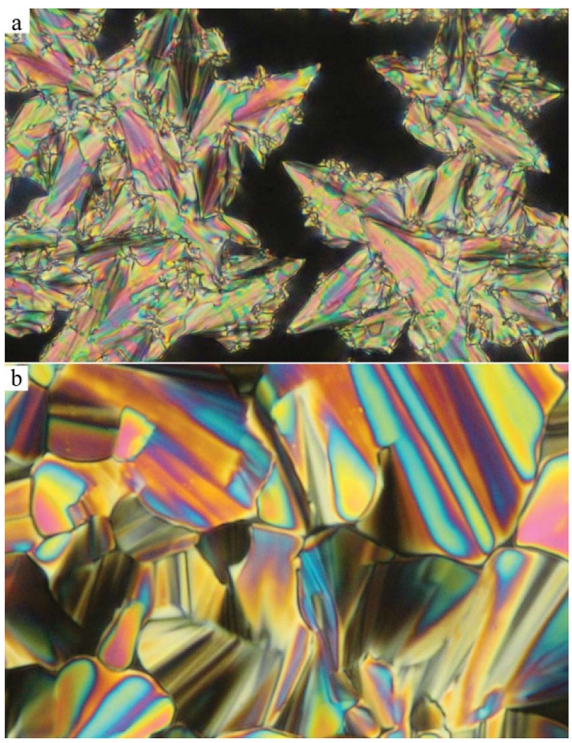

Fig. 3 (a) Planar texture of **D4-6** at the isotropic–SmA phase transition at the temperature $T = 159$ °C; (b) planar texture of **D4-8** in the B_1 phase transition at the temperature $T = 130$ °C. The width of the images is 200 μm.

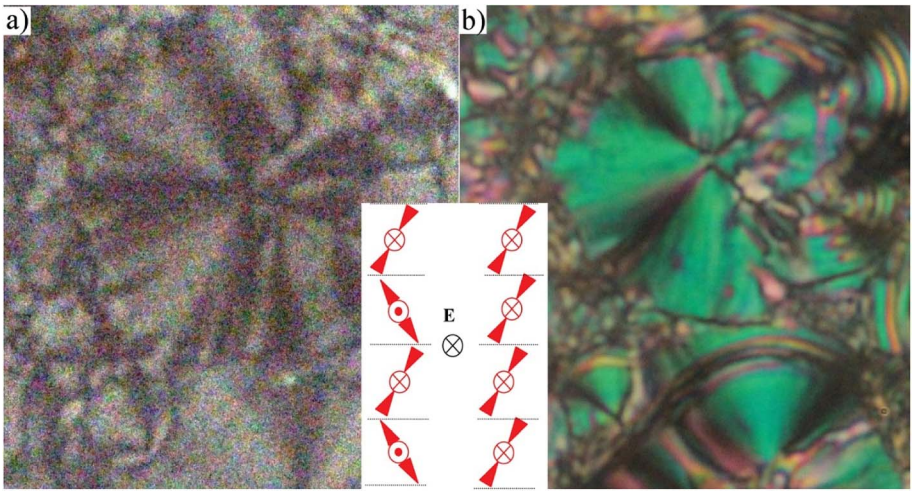

Fig. 4 The planar texture for **D4-10** at $T = 100\ ^{\circ}C$: (a) after application of the electric field (in increased contrast), and (b) in the electric field 20 V μm^{-1}. The width of the photo corresponds to about 100 μm. In the inset the schematic organization of bent-core molecules is shown in a homochiral domain without electric field (left column) and under the applied electric field E (right column), when the average extinction turns for about 45 degrees.

from C_2H_5 to $C_{12}H_{25}$. The aim is to compare their behaviour with the previous results[28] and obtain more information about molecular structure–mesomorphic properties relationship.

The phase sequence, the transition temperatures and corresponding enthalpy changes for this series are summarized in Table 1. DSC plots for selected homologues are presented in

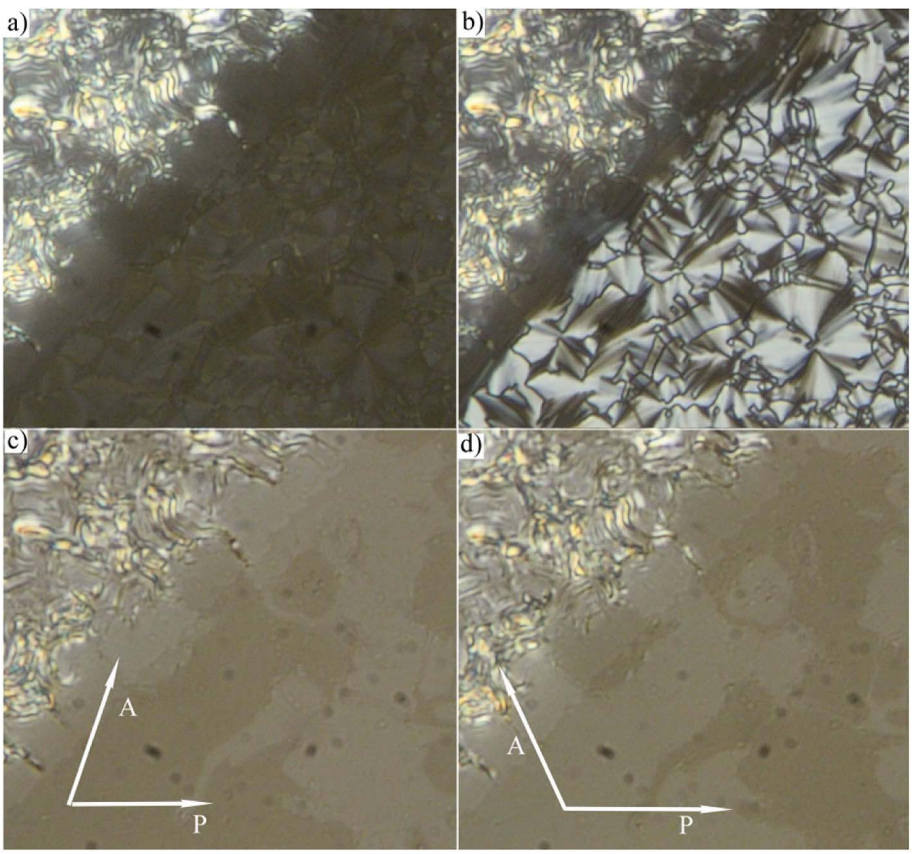

Fig. 5 Planar texture of **D4-12** in the SmCP phase at $T = 130\ ^{\circ}C$: (a) the texture when the field was switched off and upper left part of the photo show the virgin texture out of the electrode (b) in the applied electric field 10 V μm^{-1}. For (a) and (b) the polarizer (P) and the analyser (A) are in crossed position; (c) and (d) show the same texture as in (a) when rotation the analyser clockwise and anticlockwise. The width of every figure corresponds to 150 μm.

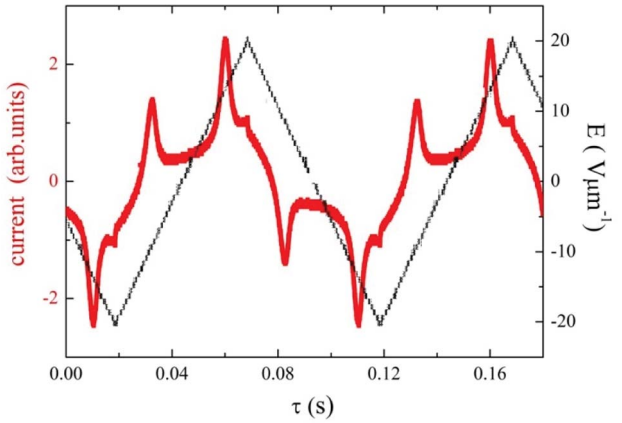

Fig. 6 For D4-12, the switching current *versus* time, τ, for applied triangular voltage with intensity, E, at a frequency of 10 Hz, taken in the SmC_AP_A at $T = 120$ °C.

Fig. 2. Compounds **D4-2** to **D4-6** with the shortest alkyl chains exhibited the SmA phase. Fan-shaped texture has been found under polarizing microscope and no electro-optical response to the applied electric field has been detected. We consider the observed mesophase is a non-polar SmA phase, on contrary to polar SmAP phases described in literature.[29] Due to the strong intercalation any switching in the electric field is blocked. For **D4-6** the grow of the nuclei of the SmA phase at the Iso–SmA phase transition is presented in Fig. 3a. The developed planar texture in the SmA phase is demonstrated for **D4-2** in ESI, Fig. S1.† The homologue **D4-8** showed a columnar phase and typical textures with coloured domains were observed under polarizing microscope (Fig. 3b). Also for the columnar phase no electro-optical response was detected.

To confirm the LC phase identification based on textural observations, X-ray measurements were performed. X-ray pattern recorded in the SmA phase, with the sharp commensurate peaks at small-angle region and broad diffuse maximum at wide range of scattering angle, is typical for a lamellar phase with liquid-like positional order within the layers. Comparison between the measured layer spacing value, $d = 16.7$ Å for **D4-2**, and estimated molecular length $L = 33.6$ Å evidences a strongly intercalated character of the observed SmA mesophase. Analogously we have also proved the intercalated structure of SmA phases for longer homologues, **D4-4** and **D4-6**. The broad diffuse maximum in the X-ray pattern corresponds to average in-plane distance of molecules about 4.5 Å.

In the X-ray pattern of the columnar phase formed by **D4-8**, there are few incommensurate signals in the small-angle region and diffuse maximum at wide scattering angle. The pattern could be indexed assuming centred orthorhombic crystallographic unit cell, that identifies B_1-type columnar mesophase, which structure is built from smectic-layer fragments.[5] The unit cell dimensions were established and we found that parameter c is comparable to the molecular length (see Table S1 in ESI†). The cell parameters for **D4-8** are very similar to values presented for the propylenedioxy compounds **D3-6** and **D3-8**.[28] Thus, we can claim that the packing scheme of broken-layer fragments in the B_1 phase presented for dimers **D3-n** in our preliminary paper is valid also for the analogues **D4-n** studied here.

For compounds **D4-10** and **D4-12** we have observed another type of the mesophase. **D4-10** and **D4-12** showed an electro-optical response and other features characteristic for SmCP phases. Virgin planar textures show very tiny features, however under the applied electric field a fan-shaped texture with circular domains appeared (Fig. 4) After switching off the electric field, the fan-shape texture turned to dark state with the extinction positions corresponding to the polarizers direction (Fig. 4a). The birefringence is very low and the contrast should be increased to recognize the fans. Under the applied electric field the extinction positions rotate by angle about 45 degrees and the birefringence increases with voltage (Fig. 4b). Fig. 5 shows the texture behaviour for homologue **D4-12** after application of the applied electric field (Fig. 5a) and under the field (Fig. 5b); the left upper corner of each panel shows the virgin texture in area, which is not covered by the electrode. By rotating the polarizer from crossed position by an angle of about 7 degrees clockwise and anticlockwise, one can easily distinguish large domains (Fig. 5c and d), which corresponds homochiral state. We can conclude that the textures and

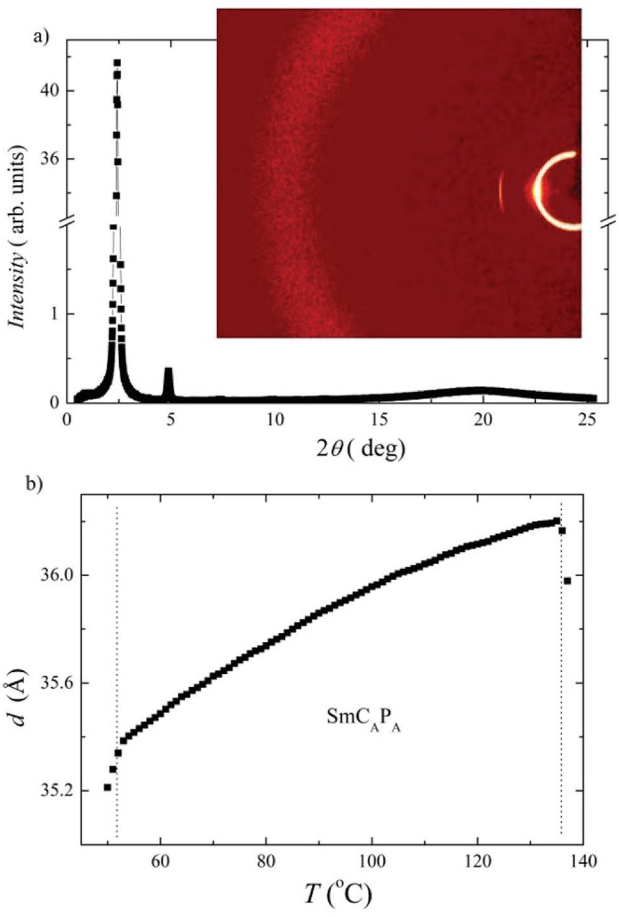

Fig. 7 X-ray measurements for compound D4-12: (a) the intensity *versus* the scattering angle at $T = 70$ °C in the SmC_AP_A phase. In the inset in right upper corner 2D X-ray pattern is shown at the same temperature; (b) temperature dependence of the layer spacing, d, taken on cooling.

Table 2 Mesomorphic properties of dimers **Dm-12** taken from DSC measurements[a]

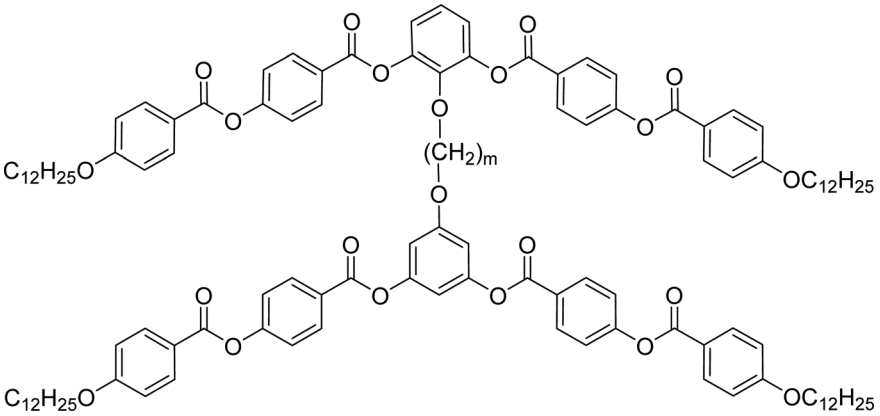

Comp.	*m*	mp [Δ*H*]	T_{cr} [Δ*H*]	M_1	T_{tr} [Δ*H*]	Iso
D2-12	2	103 [+40.6]	85 [−34.1]	SmC_AP_A	183 [−45.4]	•
D3-12[24]	3	129 [+37.3]	99 [−25.3]	SmC_AP_A	139 [−39.4]	•
D4-12	4	102 [+36.8]	49 [−25.5]	SmC_AP_A	134 [−40.4]	•
D5-12	5	72 [+28.8]	*	SmC_AP_A	94 [−41.0]	•
D6-12	6	120 [+98.1]	106 [−102.8]	—	—	•
D8-12	8	118 [+136.2]	107 [−90.9]	—	—	•
D12-12	12	108 [+104.3]	91 [−123.2]	—	—	•

[a] Melting point, mp, phase transition temperatures, T_{tr}, and temperature of crystallization, T_{cr}, in °C, and corresponding enthalpy changes, Δ*H*, in kJ mol^{-1}, taken on the second heating/cooling run are in brackets. Symbol * shows that compound does not crystallise on cooling to −20 °C.

Table 3 Mesomorphic properties of dimers **Dm-1212-FF**, **Dm-FF-FF**, **D3-12F-12F**, **D3-11F-11F**, **D3-SiF-SiF**[a]

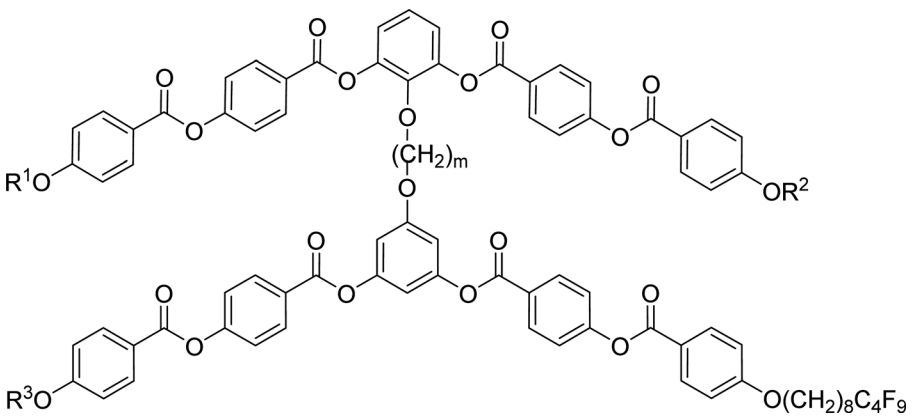

Comp.	*m*	R^1	R^2	R^3	mp [Δ*H*]	T_{cr} [Δ*H*]	M_1	T_{tr} [Δ*H*]	Iso
D2-1212-FF	2	$C_{12}H_{25}$	$C_{12}H_{25}$	$(CH_2)_8C_4F_9$	90 [+31.5]	66 [−19.6]	SmC_AP_A	202 [−44.4]	•
D3-1212-FF	3	$C_{12}H_{25}$	$C_{12}H_{25}$	$(CH_2)_8C_4F_9$	114 [+44.7]	70 [−22.8]	SmC_AP_A	160 [−38.3]	•
D4-1212-FF	4	$C_{12}H_{25}$	$C_{12}H_{25}$	$(CH_2)_8C_4F_9$	89 [+30.4]	*	SmC_AP_A	156 [−39.4]	•
D5-1212-FF	5	$C_{12}H_{25}$	$C_{12}H_{25}$	$(CH_2)_8C_4F_9$	123 [+39.4]	*	SmC_AP_A	120 [−34.1]	•
D3-FF-FF	3	$(CH_2)_8C_4F_9$	$(CH_2)_8C_4F_9$	$(CH_2)_8C_4F_9$	84 [+28.7]	*	SmC_AP_A	187 [−42.5]	•
D4-FF-FF	4	$(CH_2)_8C_4F_9$	$(CH_2)_8C_4F_9$	$(CH_2)_8C_4F_9$	86 [+37.3]	64 [−28.7]	SmC_AP_A	180 [−38.8]	•
D3-12F-12F	3	$C_{12}H_{25}$	$(CH_2)_8C_4F_9$	$C_{12}H_{25}$	113 [+37.2]	76 [−22.5]	SmC_AP_A	182 [−40.1]	•
D3-11F-11F	3	$(CH_2)_9CH{=}CH_2$	$(CH_2)_8C_4F_9$	$(CH_2)_9CH{=}CH_2$	82 [+45.4]	72 [−15.6]	SmC_AP_A	154 [−35.9]	•
D3-SiF-SiF	3	$(CH_2)_{11}SiMe_2OSiMe_3$	$(CH_2)_8C_4F_9$	$(CH_2)_{11}SiMe_2OSiMe_3$	62 [+29.2]	71 [−13.0]	SmC_AP_A	162 [−40.3]	•

[a] Melting point, mp, phase transition temperatures, T_{tr}, and temperature of crystallization, T_{cr}, in °C, and corresponding enthalpy changes, Δ*H*, in kJ mol^{-1}, are in brackets. Symbol * shows that compound does not crystallise on cooling down to −20 °C.

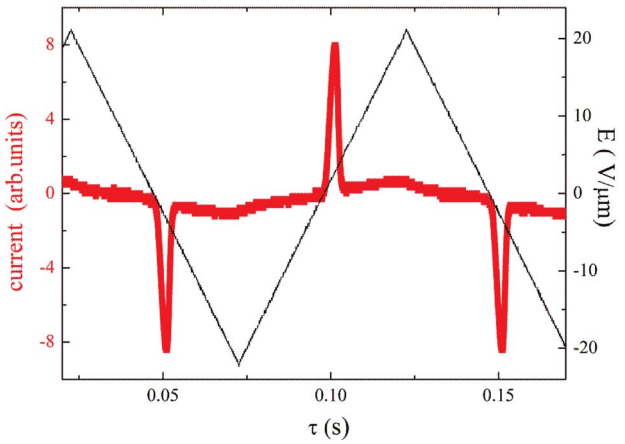

Fig. 8 For **D3-SiF-SiF**, the switching current *versus* time, τ, for applied triangular voltage profile with maximum intensity $E = 20$ V μm^{-1}, taken in the SmC_AP_A at $T = 120$ °C and a frequency of 10 Hz.

characteristic electro-optical behaviour allowed identification of the observed mesophases with the SmC_AP_A phase.

Under applied electric field of a triangular profile, two peaks per half cycle have been detected, which confirms the antiferroelectric character of the observed SmCP mesophase. For **D4-12** the switching current profile is shown in Fig. 6. The spontaneous electric polarization values, calculated by integration of the current profile, slightly increased on cooling for both **D4-10** and **D4-12** compounds, being in range 800–850 nC cm^{-2}. Dielectric spectroscopy, performed in the frequency range 10Hz to 1MHz revealed one distinct relaxation mode, which existed only within temperature interval of the SmC_AP_A phase and disappeared in the isotropic and crystalline phases (Fig. S2 in ESI†).

X-ray diffraction measurements have been performed for **D4-10** and **D4-12** to confirm the lamellar character of the SmC_AP_A phase. X-ray intensity profile shows several commensurate peaks in small angle region, from which the layer spacing, d, can be calculated. For compound **D4-12** the intensity profile and temperature dependence of the layer spacing $d(T)$ are presented in Fig. 7a. The layer spacing decreases on cooling for both studied compounds, for **D4-12** $d(T)$ is presented in Fig. 7b. Comparison of the calculated length of the **D4-10** and **D4-12** molecules on extended conformation with the measured d values, suggest very high tilt angle value, ~50 degrees. Thus it is reasonable to assume that interdigitation of molecular terminal chains between neighbouring layers also takes place and contributes to lowering the effective smectic layer thickness.

The above described mesomorphic properties of the series **D4-n** compounds, having the butylenedioxy spacer are very similar to those observed for compounds **D3-n** with the propylenedioxy spacer.[28] We have not observed typical odd/even effect of the spacer parity on the phase transition temperatures or mesomorphic behaviour for studied top-to-bottom dimers.

The role of the length of the alkylenedioxy spacer

Furthermore, we studied the role of the spacer length (m number, see Fig. 1) and prepared a series of dimers **Dm-12** with dodecyl terminal chains (Table 2) to support the polar packing. We have discovered that regardless the length and parity of atoms in the spacer, all prepared dimers **D2-12** to **D5-12** exhibited the SmCP phase, which was identified as the chiral SmC_AP_A phase. Compound **D3-12** was already reported[28] and is included into Table 2 for comparison with other homologues. Further lengthening of the spacer from 6 atoms for compounds **D6-12** to 12 carbon atoms **D12-12** led to disappearance of mesophases (for details see ESI†).

The electro-optical behaviour of the SmC_AP_A phase of all **Dm-12** compounds was found analogous to that described above for compounds **D4-10** and **D4-12**. We have evaluated the layer spacing values by X-ray measurements. For compound **D5-12** the results are presented in ESI in Fig. S3,† where the intensity *versus* the scattering angle at $T = 35$ °C and the temperature dependence of the layer spacing, d, are shown. The layer spacing for **D5-12** (34.5–35 Å) is only slightly smaller than d value found for **D4-12** (Fig. 7). This can be connected with differences in tilt angle and/or modification of the overall dimer shape. Very small decrease of the layer spacing value on cooling for **D4-12** can be explained with a slight increase of the molecular tilt in the SmC_AP_A phase.

Modification of the terminal chains

Furthermore we changed the polar character of the terminal chain by introduction polyfluoroalkyl (9,9,10,10,11,11,12,12,12-nonafluorododecyl) and siloxanylalkyl (11-(1,1,3,3,3)-pentamethyldisiloxanyl)undecyl chains to design materials **Dm-1212-FF**, **Dm-FF-FF**, **D3-12F-12F**, **D3-11F-11F**, **D3-SiF-SiF** (Table 3). The motivation was to modify the self-assembly process and polar packing of the investigated dimers.[30–34] At first, a series of materials **Dm-1212-FF** (m = 2–5) was prepared, in which the upper bent-unit possesses the dodecyl terminal chains

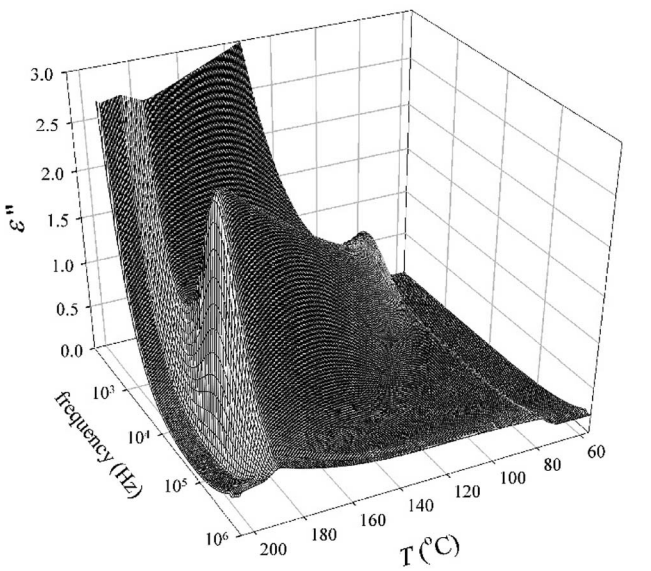

Fig. 9 Three-dimensional plot of the imaginary part of dielectric permittivity, ε'', *versus* temperature, T, and frequency in the SmC_AP_A phase for **D3-FF-FF**.

Table 4 Mesomorphic properties of dimers **Dm-12/3**[a]

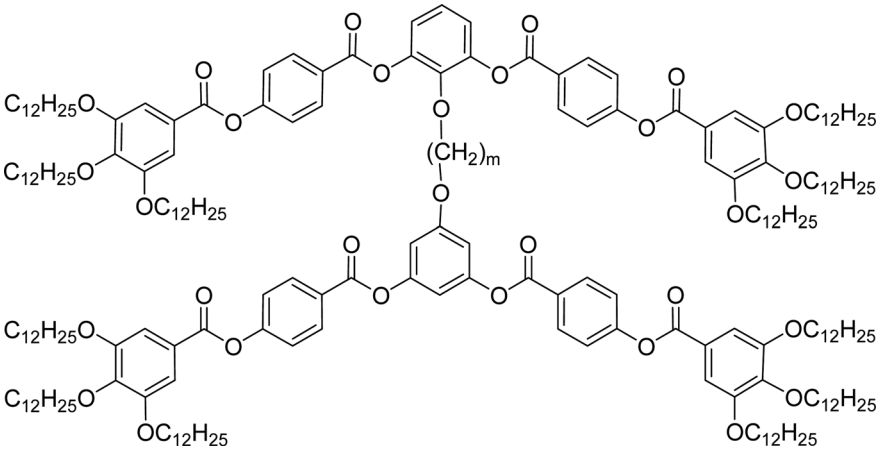

Comp.	m	mp [ΔH]	T_{cr} [ΔH]	M_1	T_{tr} [ΔH]	Iso
D3-12/3	3	−30 [+36.4]	−7 [−37.4]	Col_h	45 [−4.4]	•
D4-12/3	4	−30 [+31.5]	−8 [−40.5]	Col_h	43 [−3.9]	•

[a] Melting point, mp, phase transition temperatures, T_{tr}, and temperature of crystallization, T_{cr}, in °C, and corresponding enthalpy changes, ΔH, in kJ mol^{-1}, detected on the second temperature run at a rate of 5 K min^{-1} are in brackets.

(symmetrically in both arms), while the bottom unit was terminated with a polyfluoroalkyl units. At the same time the distance between bent-core units was modified by changing the length of the alkylenedioxy spacer (m = 2–5). Compounds are formally symmetrical along the vertical axis. In spite of our strategy, such structural change did not exert a substantial influence on mesomorphic properties in comparison with materials **Dm-12** (Table 2) and all materials exhibited the SmCP phase. The mesomorphic behaviour is summarized and compared in Table 3. Presence of two polyfluoroalkyl chains resulted in the increase of transition temperatures and the mesophase stability range. When all the dodecyl terminal chains were fully replaced by polyfluoroalkyl chains in compounds **Dm-FF-FF** (m = 3,4) further rise of clearing temperatures and stabilization of the SmCP phase is proved (Table 3) in comparison with compounds **Dm-12**.

Other type of asymmetry was introduced into the dimers when both the upper and bottom units were terminated with different chains. We have utilized dodecyl/polyfluoroalkyl in **D3-12F-12F**, undecenyl/polyfluoroalkyl in **D3-11F-11F**, and pentamethyldisiloxane undecyl/polyfluoroalkyl chains in **D3-SiF-SiF**. However, regardless the change in character of the terminal chains, the materials kept their phases and all prepared homologues exhibited broad SmC_AP_A phases with small shifts in the phase transition temperatures only. Selected DSC thermographs are presented in ESI (Fig. S4)† for illustration. Compounds **D4-1212-FF**, **D5-1212-FF** and **D3-FF-FF** did not crystallise on cooling during DSC measurements but crystallised on subsequent heating run. It is visible as an opposite peak on the heating curve (Fig. S4a†).

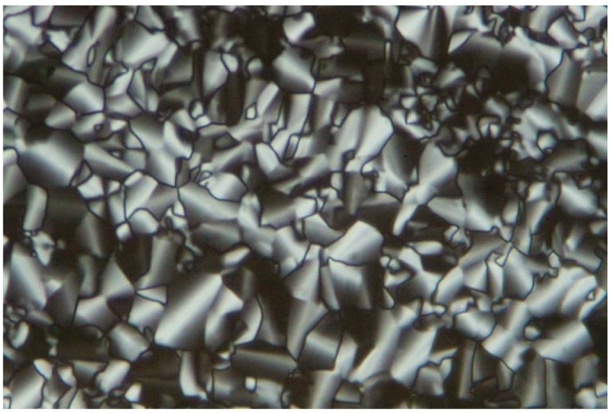

Fig. 10 Texture of **D3-12/3** at T = 30 °C. The width of the figure corresponds to 300 μm.

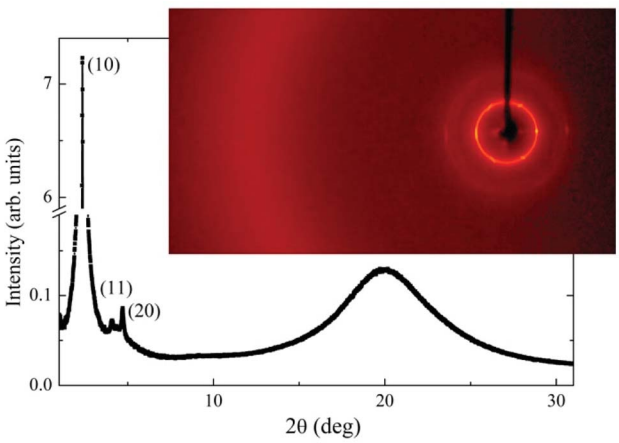

Fig. 11 Intensity of the X-ray signal *versus* scattering angle in a wide range for **D3-12/3** at T = 25 °C in the Col_h phase. In the inset 2D X-ray pattern is shown at the same temperature.

Table 5 Mesomorphic properties of dimers with modified linking groups[a]

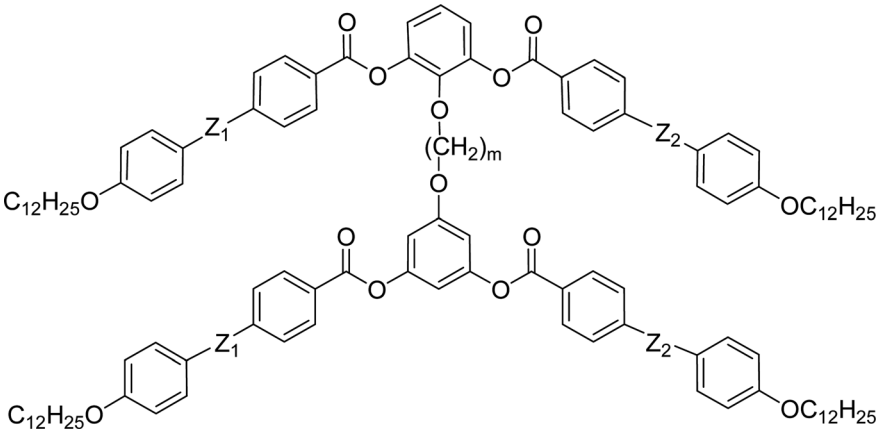

Comp.	m	Z_1	Z_2	mp [ΔH]	T_{cr} [ΔH]	M_1	T_{tr} [ΔH]	Iso
D3-12/inv	3	OOC	COO	118 [+40.2]	100 [−10.3]	SmC_AP_A	201 [−31.0]	•
D4-12/inv	4	OOC	COO	119 [+28.4]	98 [−24.7]	SmC_AP_A	190 [−38.9]	•
D3-12/azo	3	N=N	N=N	140 [+52.4]	109 [−32.0]	SmC_AP_A	149 [−30.5]	•
D4-12/azo	4	N=N	N=N	137 [+60.5]	101 [−32.2]	SmC_AP_A	142 [−24.5]	•
D3-12/Ph2	3	—	—	150 [+44.9]	144 [−22.0]	SmC_AP_A	149 [−27.2]	•
D4-12/Ph2	4	—	—	134 [+36.8]	107 [−29.0]	SmC_AP_A	139 [−34.9]	•

[a] Melting point, mp, phase transition temperatures, T_{tr}, and temperature of crystallization, T_{cr}, in °C, and corresponding enthalpy changes, ΔH, in kJ mol^{-1}, are in brackets.

All the compounds listed in Tables 2 and 3 exhibited the SmC_AP_A mesophase with similar electro-optical behaviour, and can be described together. Textures and their behaviour in the applied electric field were described above for **D4-10** and **D4-12** (Fig. 4–6). The only difference concerns the threshold voltage, E_{th}, at which the electro-optical changes can be observed. E_{th}, for fluorinated compounds **Dm-1212-FF** and **Dm-FF-FF** is about 10 V μm^{-1}, which is lower in comparison with $E_{th} \approx 15$ V μm^{-1} for **D4-10** and **D4-12**. Very small threshold voltage, $E_{th} \approx 2$ V μm^{-1}, was found for compound with oligosiloxane units in the terminal chain, **D3-SiF-SiF**. Switching current for **D3-SiF-SiF** reveals only on distinct peak per half period of applied voltage, as it is shown in Fig. 8, which results from overlap of the signals coming from two consecutive switching events. Polarization values have been evaluated 800–1000 nC cm^{-2} for compounds from Table 3. Dielectric spectroscopy performed for **D3-SiF-SiF** (see Fig. S5†) and **D3-FF-FF** (Fig. 9) showed that the dielectric behaviour exhibits very similar features to other presented compounds with the SmC_AP_A phase (see Fig. S2† for **D4-10**). It evidences of the similar type of structures and arrangement of molecules in all observed tilted lamellar mesophases.

The X-ray measurements were performed for all compounds from Table 3 and the tilted lamellar mesophase presence was confirmed. Due to analogy with compounds studied above (see Fig. 7), the results are summarized in ESI.† In Fig. S6† the X-ray measurements is demonstrated for compound **D4-1212-FF**, which exhibits the layer spacing, d, decreasing on cooling from 38.8 Å to 36.9 Å. In Fig. S7,† the X-ray intensity *versus* scattering angle is presented in 2D picture for **D3-11F-11F** at $T = 100$ °C and layer spacing was established 38.7 Å. Similar temperature behaviour and layer spacing values have been detected for other compounds. Only for compound **D3-SiF-SiF**, $d(T)$ values slightly increases on cooling and reaches higher values than other compounds ($d \approx 42$ Å). Temperature dependence $d(T)$ for **D3-SiF-SiF** is presented in ESI (Fig. S8).† The length of the molecule for **D3-SiF-SiF** has been calculated and found to be about 56.5 Å, which corresponds to the tilt angle 42 deg.

Modification of the number of terminal chains

Additionally, we have made an attempt to increase the size and/or modify the shape of the dimer by joining three alkyl chains to the terminal rings to mimic a polycatenar system. The dimers **D3-12/3** and **D4-12/3** (Table 4) decorated with dodecyl alkyl chains exhibited interesting mesomorphism. The compounds are low-melting and show a hexagonal columnar phase. Planar texture is presented in Fig. 10 for a non-aligned cell without surfactant. The sample is sensitive to shearing and textures can be aligned in this way (see Fig. S9 in ESI†).

X-ray measurements have been performed to confirm the phase identification and establish the structural parameters of the columnar phase. Presence of three sharp low-angle signals, which positions in q-space are in sequence 1:sqrt(3):2 (Fig. 11) confirms the hexagonal arrangement of columns. For both compounds, **D3-12/3** and **D4-12/3**, the lattice parameter, a, which is a measure of column diameter, was found comparable (Table S2 in ESI†).

Modification of the polar linkages

A typical modification of the bent-core liquid crystal structure involves change of the polar linkages within the molecular

arms.[1] In this respect, for materials with propylenedioxy and butylenedioxy spacers with uniform dodecyl terminal chains we reoriented the ester linkages in the outer positions of arms in materials **Dm-12/inv**. Further, we have substituted the ester linkage for azo moieties in **Dm-12/azo**. Finally, we have also removed the ester groups completely to form rigid biphenyl units in the arms for **Dm-12/Ph2** (Table 5).

Reorientation of ester groups in the ester based materials **Dm-12/inv** (Z_1=COO, Z_2=OOC) does not disturb formation of the SmC_AP_A, moreover the increase of the Iso–SmCP transition temperatures for more than 45 K with respect to parent compounds **D3-12** and **D4-12**, has been observed. Replacement for a more rigid azo linking groups (**Dm-12/azo**, Z_1=Z_2=N=N) also preserved the mesomorphic behaviour and formation of the SmC_AP_A phases was observed, however in narrower temperature intervals. Finally, the same mesomorphic behaviour was observed also for materials with biphenyl units in the side arms (**Dm-12/Ph2**), where still narrower SmC_AP_A phases were found. The DSC thermographs for selected compounds from this series are presented in ESI (Fig. S10).† The performed X-ray measurements confirmed the lamellar character of mesophase in all modified compounds. Additionally, we have studied electro-optical properties to establish polar character of the SmC_AP_A phase. We can conclude that the character and electro-optical response of the SmC_AP_A phase remains unchanged. Dielectric spectroscopy data evidencing polar mode is presented in ESI (Fig. S11 for **D4-12/inv**).† Imaginary part of permittivity, ε'', shows distinct maxima at a frequency of about 10 kHz. Switching current with characteristic profile with two peaks in half-cycle is presented in ESI for **D4-12/Ph2** (Fig. S12).† Polarization values have been calculated $P_S \approx 700$–900 nC cm^{-2} for compounds listed in Table 5. In conclusion, increasing the rigidity of the lengthening arms resulted in narrowing the interval of SmCP phases.

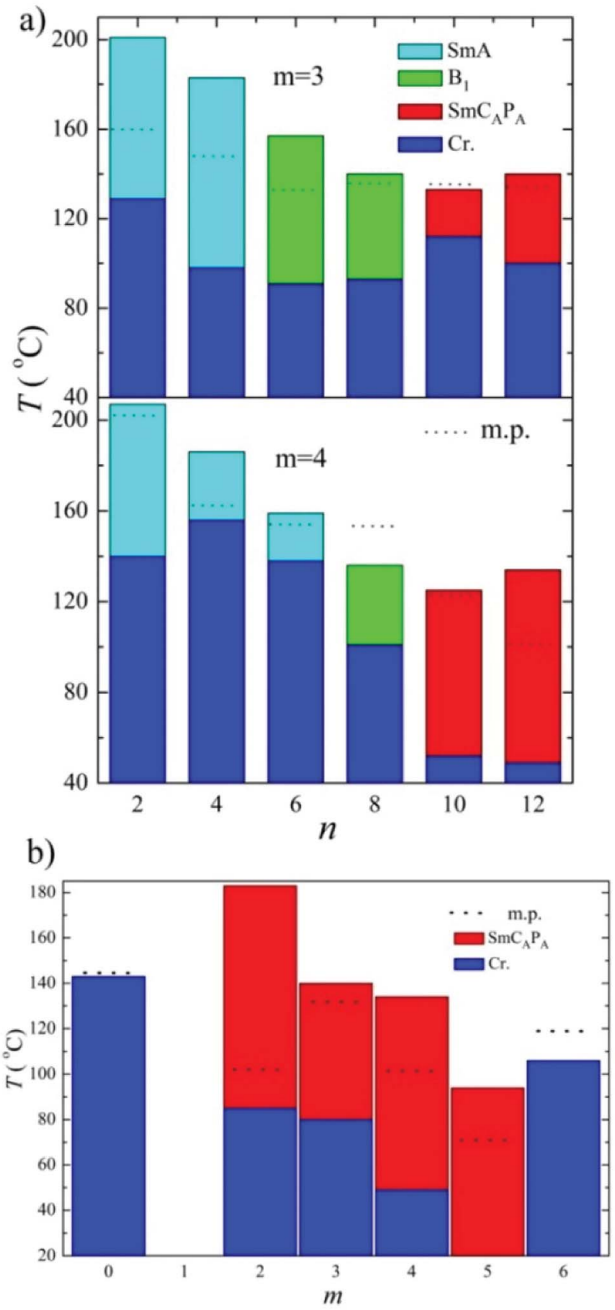

Fig. 12 Effect of spacer length (m) on mesomorphic properties: (a) phase transition temperatures and phases *versus* terminal chain length (n) for $m = 3$ and $m = 4$, (b) *versus* the spacer length (m) for compounds **Dm-12**.

Discussion and conclusions

To summarize, we have found that the character of mesophase exhibited by top-to-bottom bent-core dimers strongly depends on the length of terminal chains. The shortest homologues exhibit the SmA phase, for the average terminal chain length a columnar B_1 phase is formed and while the longest homologues reveal switchable lamellar mesophases. The butylenedioxy homologues **D4-n** exhibited the intercalated SmA phase for $n = 2$, 4 and 6. We should stress that all observed SmA phases reveal similar character: SmA is non-polar orthogonal phase with the layer spacing value close to half-length of the molecule, which evidences deep intercalation for this type of phase. Such a phase is non-switchable and does not respond to applied electric field. For propylenedioxy derivative **D3-6** the columnar B_1 phase was reported, on contrary, **D4-6** shows the SmA phase. In the columnar B_1 phase with a structure of "broken-layers" the dimeric molecules are more organized that in the SmA phase. One can conclude the lengthening of the spacer for $n = 6$ disturbs packing of molecules and a less ordered phase is preferred.

The effect of the terminal chain length (n number) for series **D3-n** and **D4-n** is presented in Fig. 12a. For long terminal chains, $n = 10$ and 12, we have observed the switchable SmC_AP_A phase, characteristic for bent-core monomeric mesogens. For all studied mesogens with SmC_AP_A phase the physical properties are similar and can be described together. The ground state is anticlinic, as is clearly demonstrated in planar textures by optical extinction oriented along the smectic layer normal (along the fan symmetry-axis). Under applied electric filed the extinction position rotates and reveals inclination from the ground position, which corresponds to transformation into

synclinic state under the field. Such behaviour is characteristic for SmC_AP_A–SmC_SP_F transformation in the electric field for bent-core compounds.[2] From this type of electro-optical behaviour we can imagine the dimer response to the electric field in a similar manner as is described for bent-core molecules.

For terminal chain $n = 12$ we have found that up to the spacer length $m = 5$ we can observe mesogenic properties, the above described SmC_AP_A phase. For compounds with $m \geq 6$ mesomorphic properties are lost, which is obviously caused by larger mutual independence of the single bent units and change of supramolecular packing. In Fig. 12b it is demonstrated the shift of the temperature interval of the SmC_AP_A phase to lower temperatures with increasing m value. We found that there is no typical odd/even effect of the spacer parity on the mesomorphic properties for studied type of dimers.

One of the important requirements for the formation of bent-core phases is the microsegregation of the rigid polar bent-core structure from the terminal and less polar alkyl groups.[1] The extent of microsegregation can be modified by introduction of different chains, *e.g.*, polyfluoroalkyl and oligosiloxane units, which are incompatible with alkyl and aromatic units, respectively. Generally, for simple bent-core molecules the presence of the fluorinated chains[31–33] causes the broadening and stabilization of lamellar phases and increase of clearing temperatures. To modify the mesogenic properties of switchable SmCP phases for the present study of top-to-bottom dimers, we concentrated on long terminal chains and varied their structure. Fluorination of terminal chains did not substantially affect the mesophase character. Nevertheless, compound **D3-SiF-SiF** with the siloxanylalkyl chains exhibited a very low threshold voltage for the electro-optical switching from antiferro to ferroelectric state. We can summarize that by variation of the terminal chains we have stabilized the SmC_AP_A mesophases and optimized their electro-optical properties.

Rather unique attempt to modify the structures of dimers by substituting of multiple terminal chains to outer phenyl rings led to a polycatenar system that exhibited substantially decreased transition temperatures and different type of liquid crystalline phases – instead of lamellar phases a columnar hexagonal phase was found.

Conflicts of interest

The authors declare no conflict of interest.

Acknowledgements

This work was supported by the Czech Science Foundation (project 18-14497S).

References

1 N. Gimeno and M. B. Ros, Chemical structures, mesogenic properties, and synthesis of liquid crystals with bent-core structure, in: *Handbook of Liquid Crystals*, ed. J. W. Goodby, P. J. Collings, T. Kato, C. Tschierske, H. F. Gleeson, P. Raynes, Wiley-VCH, Weinheim, 2014, 4, p. 603, and references cited therein.
2 H. Takezoe, *Top. Curr. Chem.*, 2012, **318**, 303–330.
3 A. Eremin and A. Jakli, *Soft Matter*, 2013, **9**, 615–637.
4 M. Alaasar, M. Prehm, S. Poppe and C. Tschierske, *Chem.–Eur. J.*, 2017, **23**, 5541–5556.
5 J. Szydlowska, J. Mieczkowski, J. Matraszek, D. W. Bruce, E. Gorecka, D. Pociecha and D. Guillon, *Phys. Rev. E: Stat., Nonlinear, Soft Matter Phys.*, 2003, **67**, 031702.
6 J. Verara, J. Barbera, J. L. Serrano, M. B. Ros, N. Sebastian, R. de la Fuente, D. O. Lopez, G. Fernandez, L. Sanchez and N. Martin, *Angew. Chem., Int. Ed.*, 2011, **50**, 12523.
7 S. Pan, B. Mu, Y. Zhou, Q. Li, B. Wu, J. Fang and D. Chen, *RSC Adv.*, 2016, **6**, 49556.
8 G. Dantlgraber, S. Diele and C. Tschierske, *Chem. Commun.*, 2002, 2768.
9 C. Keith, R. Amaranatha Reddy, U. Baumeister, H. Hahn, H. Lang and C. Tschierske, *J. Mater. Chem.*, 2006, **16**, 3444.
10 R. Achten, A. Koudijs, M. Giesbers, A. T. M. Marcelis, E. J. R. Sudhölter, M. W. Schroeder and W. Weissflog, *Liq. Cryst.*, 2007, **34**, 59.
11 B. Kosata, G. M. Tamba, U. Baumeister, K. Pelz, S. Diele, G. Pelzl, G. Galli, S. Samaritani, E. V. Agina, N. I. Boiko, V. P. Shibaev and W. Weissflog, *Chem. Mater.*, 2006, **18**, 691.
12 S. Radhika, B. K. Sadashiva and V. A. Raghunathan, *Liq. Cryst.*, 2013, **40**, 1209.
13 G. Shanker, M. Prehm and C. Tschierske, *J. Mater. Chem.*, 2012, **22**, 168.
14 L.-Y. Zhang, Q.-K. Zhang and Y.-D. Zhang, *Liq. Cryst.*, 2013, **40**, 1263.
15 S. Umadevi and B. K. Sadashiva, *Liq. Cryst.*, 2007, **34**, 673.
16 S. Umadevi, B. K. Sadashiva, H. N. Shreenivasa Murthy and V. A. Raghunathan, *Soft Matter*, 2006, **2**, 210.
17 N. Sebastián, N. Gimeno, J. Vergara, D. O. López, J. L. Serrano, C. L. Folcia, M. R. de la Fuente and M. B. Ros, *J. Mater. Chem. C*, 2014, **2**, 4027.
18 C. M. Hegguilustoy, M. B. Darda, R. S. Montani, B. Heinrich, B. Donnio, D. Guillon and R. O. Garay, *Liq. Cryst.*, 2015, **42**, 1013.
19 Y. Wang, H. G. Yoon, H. K. Bisoyi, S. Kumar and Q. Li, *J. Mater. Chem.*, 2012, **22**, 20363.
20 C. V. Yelamaggad, S. K. Prasad, G. G. Nair, I. S. Shashikala, D. S. S. Rao, C. V. Lobo and S. Chandrasekhar, *Angew. Chem., Int. Ed.*, 2004, **43**, 3429.
21 N. G. Nagaveni, V. Prasad and A. Roy, *Liq. Cryst.*, 2013, **40**, 1001.
22 M.-G. Tamba, B. Kosata, K. Pelz, S. Diele, G. Pelzl, Z. Vakhovskaya, H. Kresse and W. Weissflog, *Soft Matter*, 2006, **2**, 60.
23 C. V. Yelamaggad, I. S. Shashikala, G. Liao, D. S. Shankar Rao, S. K. Prasad, Q. Li and A. Jakli, *Chem. Mater.*, 2006, **18**, 6100.
24 M.-G. Tamba, U. Baumeister, G. Pelzl and W. Weissflog, *Liq. Cryst.*, 2010, **37**, 853.
25 C. V. Yelamaggad, S. A. Nagamani, S. A. Hiremath and G. G. Nair, *Liq. Cryst.*, 2001, **28**, 1009.

26 S. K. Prasad, G. G. Nair, D. S. S. Rao, C. V. Lobbo, I. S. Shashikala and C. V. Yelamaggad, *Mol. Cryst. Liq. Cryst.*, 2005, **437**, 211.
27 M. Horčic, J. Svoboda, A. Seidler, V. Kozmík, V. Novotná, D. Pociecha and E. Gorecka, *RSC Adv.*, 2016, **6**, 41972.
28 M. Horčic, J. Svoboda, V. Novotná, D. Pociecha and E. Gorecka, *Chem. Commun.*, 2017, **53**, 2721.
29 L. Guo, K. Gomola, E. Gorecka, D. Pociecha, S. Dhara, F. Araoka, K. Ishikawa and H. Takezoe, *Soft Matter*, 2011, **7**, 2895.
30 V. Novotná, M. Kašpar, V. Hamplová, M. Glogarová, L. Lejček, J. Kroupa and D. Pociecha, *J. Mater. Chem.*, 2006, **16**, 2031.
31 D. Shen, A. Pegenau, S. Diele, I. Wirth and C. Tschierske, *J. Am. Chem. Soc.*, 2000, **122**, 1593.
32 L. Kovalenko, W. Weissflog, S. Grande, G. Pelzl and I. Wirth, *Liq. Cryst.*, 2000, **27**, 683.
33 A. Kovářová, V. Kozmík, J. Svoboda, V. Novotná, M. Glogarová and D. Pociecha, *Liq. Cryst.*, 2012, **39**, 755.
34 G. Dantlgraber, A. Eremin, S. Diele, A. Hauser, H. Kresse, G. Pelzl and C. Tschierske, *Angew. Chem., Int. Ed.*, 2002, **41**, 2408.